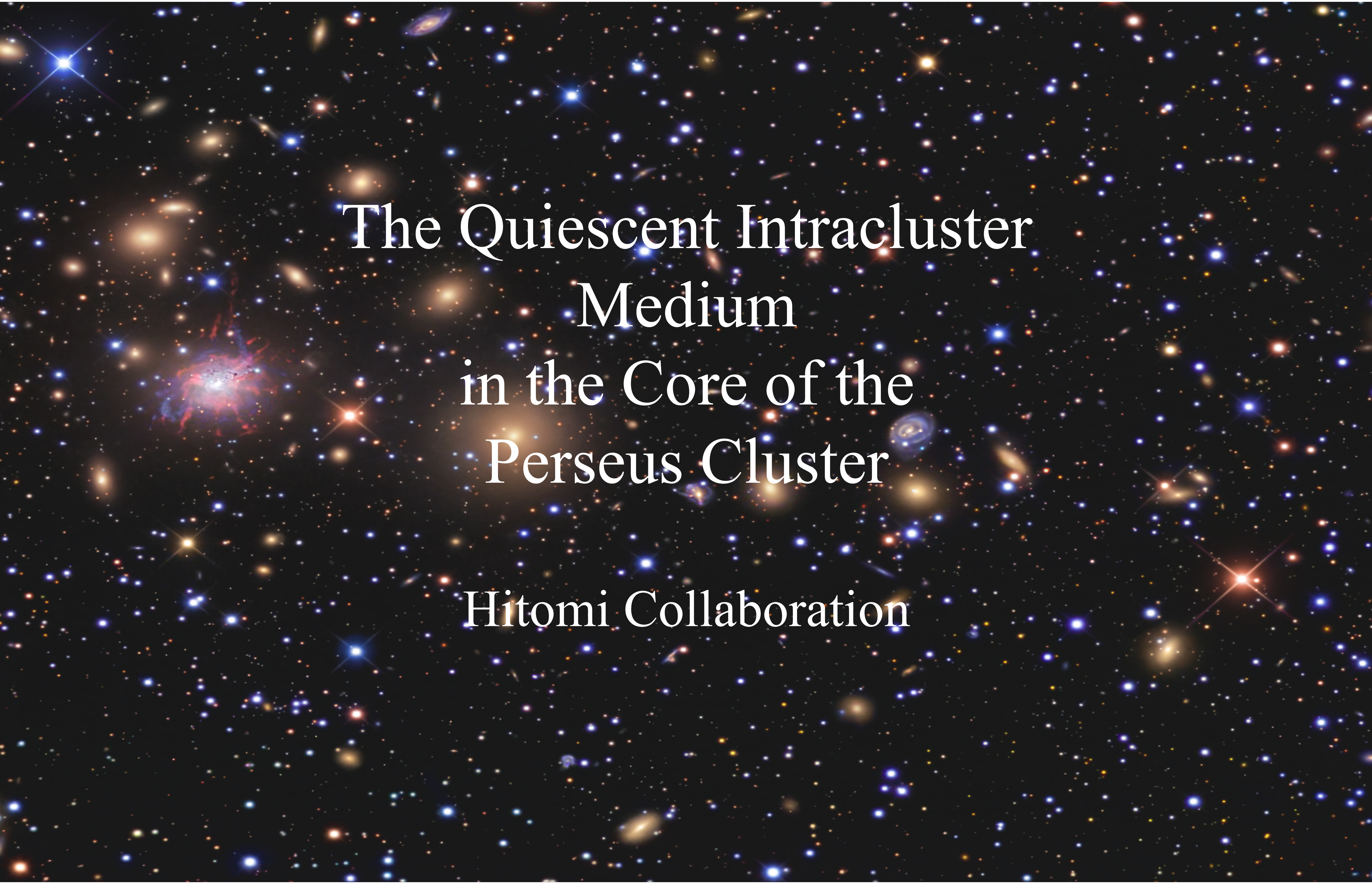

The Quiescent Intracluster Medium in the Core of the Perseus Cluster

Hitomi Collaboration

What are cluster of galaxies?

The most massive gravitationally-bound objects in the Universe

- Extent ~ 10^6 parsec
- Mass ~ 10^{14} - 10^{15} $M_\odot$

They are thus important probes of cosmological parameters and a host of astrophysical processes.

Knowledge of the dynamics of the pervasive hot gas, which dominates in mass over stars in a cluster, is a crucial missing ingredient. It can enable new insights into mechanical energy injection by the central supermassive black hole and the use of hydrostatic equilibrium for the determination of cluster masses.

X-rays from the core of the Perseus cluster are
emitted by the 50 million K diffuse hot plasma filli
its gravitational potential well. The Active Galact
Nucleus of the central galaxy NGC1275 is pumpi
jetted energy into the surrounding intracluster
medium, creating buoyant bubbles filled with
relativistic plasma. These likely induce motions in t
intracluster medium and heat the inner gas prevent
runaway radiative cooling; a process known as Acti
Galactic Nucleus Feedback. Here we report on Hito
X-ray observations of the Perseus cluster core, whi
reveal a remarkably quiescent atmosphere where t
gas has a line-of-sight velocity dispersion of 164±
km/s in a region 30-60 kpc from the central nucleu
gradient in the line-of-sight velocity of 150±70 km
is found across the 60 kpc image of the cluster co
Turbulent pressure support in the gas is 4% or less
the thermodynamic pressure, with large scale shea
most doubling that estimate. We infer that total clus
masses determined from hydrostatic equilibrium in
central regions need little correction for turbulen
pressure.

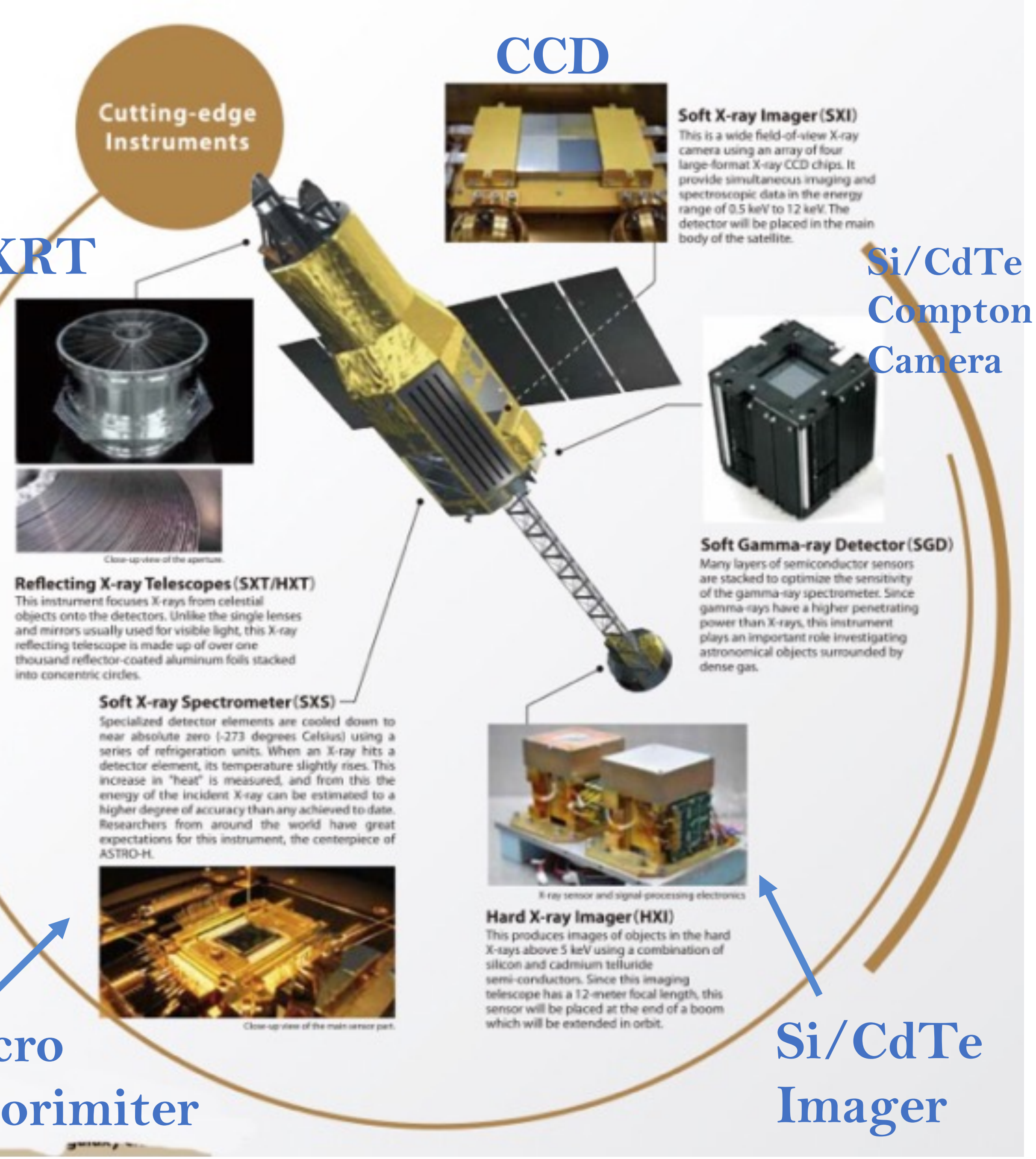

Some about JAXA Hitomi X-Ray Observa

The JAXA Hitomi X-ray Observatory was launc on 2016 February 17 from Tanegashima, Japan carries the non-dispersive Soft X-ray Spectrom SXS, which is a calorimeter cooled to 0.05K giv 4.9 eV FWHM (E/dE=1250 at 6 keV) Gaussia shaped energy response over a 6 x 6 pixel arr (total 3 x 3 arcmin). It operates over an energ range of 0.3-12 keV with X-rays focused by mirror with angular resolution of 1.2 arcmin (HPD). A gate valve was in place for early observations to minimize the risk of contamina from outgassing of the spacecraft. It includes a window that absorbs most X-rays below ~3 ke The SXS can detect bulk and turbulent motion the intracluster medium (ICM) by measuring Doppler shifts and broadening of the emission l with unprecedented accuracy. It also allows th detection of weak emission lines or absorptio features.

Short introduction to SXS work

XS imaged a 60 x 60 kpc region in the Perseus cluster centered
nin to the NW of the nucleus for a total exposure time of 230 ks.
ffset from the nucleus was due to the attitude control system
ving then been calibrated. For this early observation, not all
ation procedures were available; in particular, we did not have
mporaneous calibration of the energy scale factors (gains) of
tector pixels. Gain variation over short time intervals was
ted using a separate calibration pixel illuminated by 5.9 keV
α photons from an 55Fe X-ray source. Gain values were pinned
absolute scale via extrapolation of a subsequent calibration of
hole array 10 days later using illumination by another 55Fe
mounted on the filter wheel. (For more detail, see Methods.)
ed a subset of the Perseus data closest to that calibration to
the velocity map. For the line-width determination, we used
ll dataset to minimize the statistical uncertainty, and applied a
actor to force the Fe He-α complex from the cluster to have the
energy in all pixels. This minimizes the gain uncertainty in the
mination of the velocity dispersion but also removes any true
ions of the ICM line-of-sight velocity across the field.

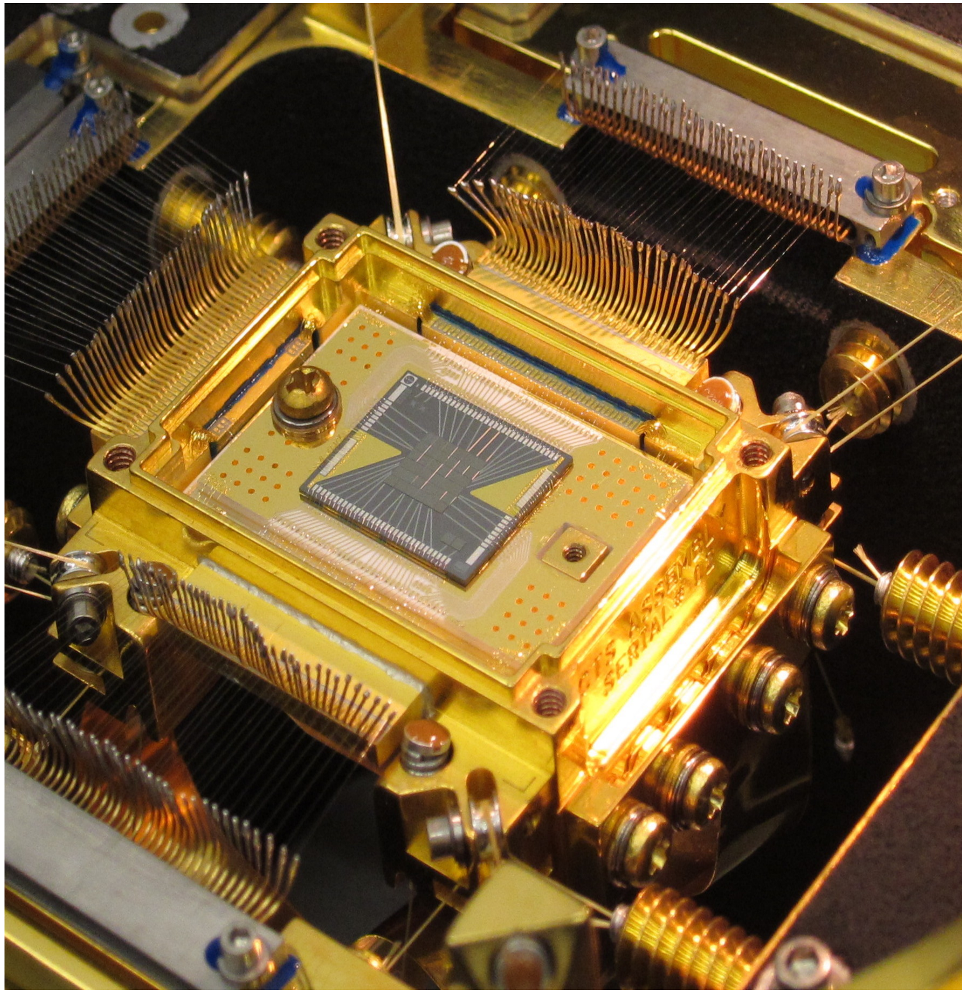

https://phonon.gsfc.nasa.gov/

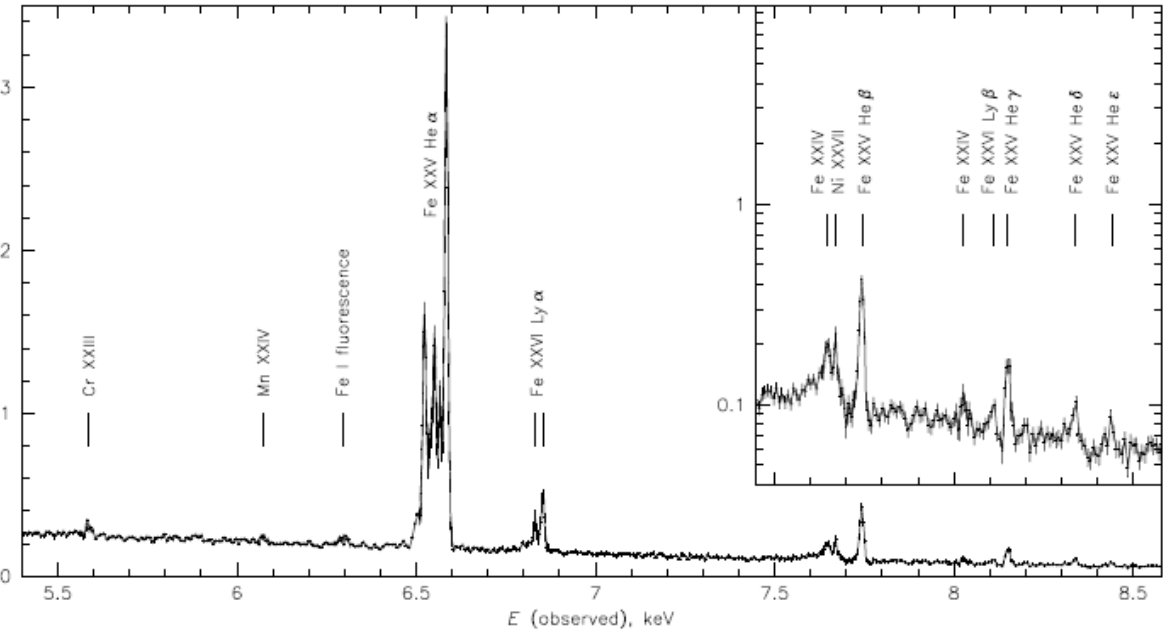

g 1 Full array spectrum of the Perseus cluster core obtained by the tomi observatory. The redshift of the Perseus cluster is 0.01756. The set above 7.5 keV has a log scale which allows the weaker lines to be tter seen.

Energy (eV)	λ (Å)	Charge state	Transition	Label	Note
He-α multiplet					
6617.00	1.8737				Blend – identifi in (35) as Be- ar Li-like iron
6628.93	1.8704	XXIII	$1s2s^2 2p\ ^1P_1 \rightarrow 1s^2 2s^2\ ^1S_0$		Be-like
6636.84	1.8681	XXV	$1s2s\ ^3S_1 \rightarrow 1s^2\ ^1S_0$	He α (z)	Forbidden
6645.24	1.8658	XXIV	$1s2p^2\ ^2D_{5/2} \rightarrow 1s^2 2p\ ^2P_{3/2}$		Li-like
6654.19	1.8633	XXIV	$1s2s2p\ ^2P_{1/2} \rightarrow 1s^2 2s\ ^2S_{1/2}$ $1s2p^2\ ^2D_{3/2} \rightarrow 1s^2 2p\ ^2P_{1/2}$		Li-like blend
6662.09	1.8610	XXIV	$1s2s2p\ ^2P_{3/2} \rightarrow 1s^2 2s\ ^2S_{1/2}$		Li-like
6667.90	1.8594	XXV	$1s2p\ ^3P_1 \rightarrow 1s^2\ ^1S_0$	He α (y)	Intercombinatio
6682.45	1.8554	XXV	$1s2p\ ^3P_2 \rightarrow 1s^2\ ^1S_0$	He α (x)	Intercombinatio
6700.76	1.8503	XXV	$1s2p\ ^1P_1 \rightarrow 1s^2\ ^1S_0$	He α (w)	Resonance
H-like doublet					
6951.96	1.7834	XXVI	$2p\ ^2P_{1/2} \rightarrow 1s\ ^2S_{1/2}$	Ly α2	
6973.18	1.7780	XXVI	$2p\ ^2P_{3/2} \rightarrow 1s\ ^2S_{1/2}$	Ly α1	
He-β doublet					
7871.31	1.5751	XXV	$1s3p\ ^3P_1 \rightarrow 1s^2\ ^1S_0$	He β2	
7880.67	1.5733	XXV	$1s3p\ ^1P_1 \rightarrow 1s^2\ ^1S_0$	He β1	

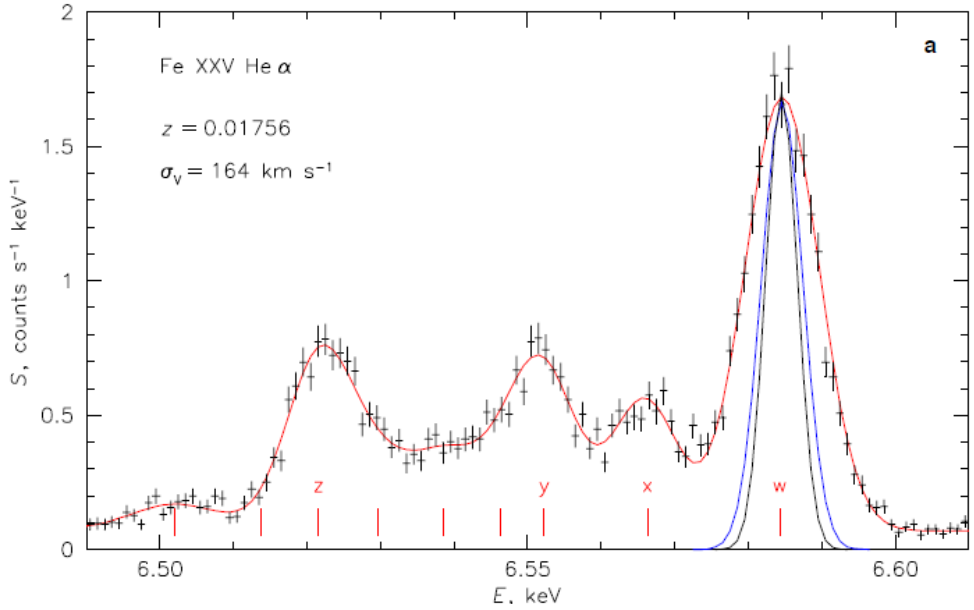

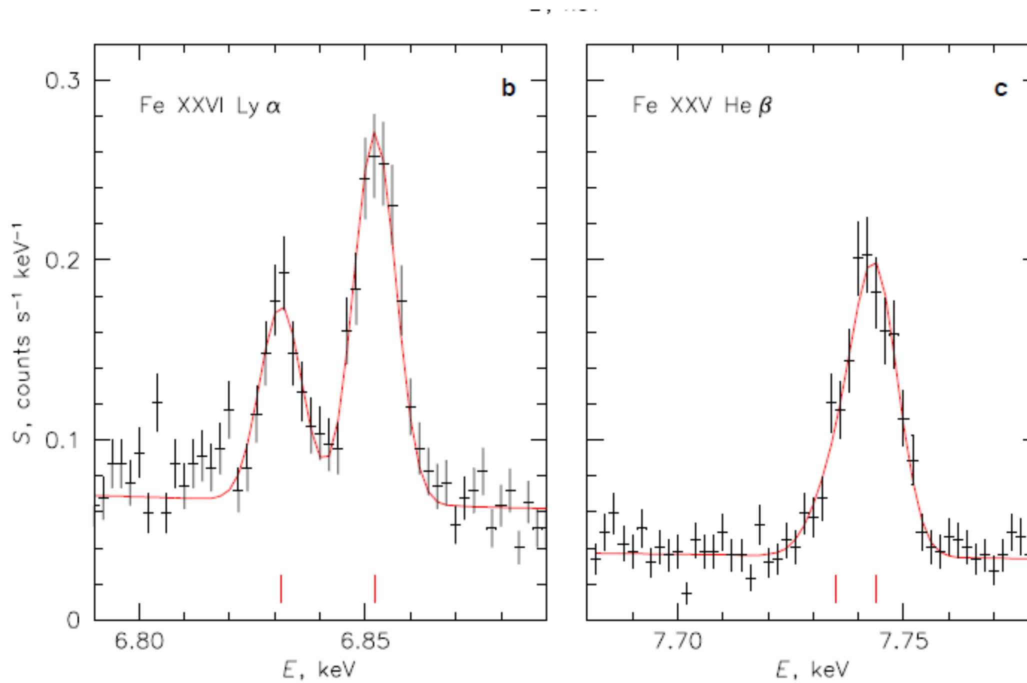

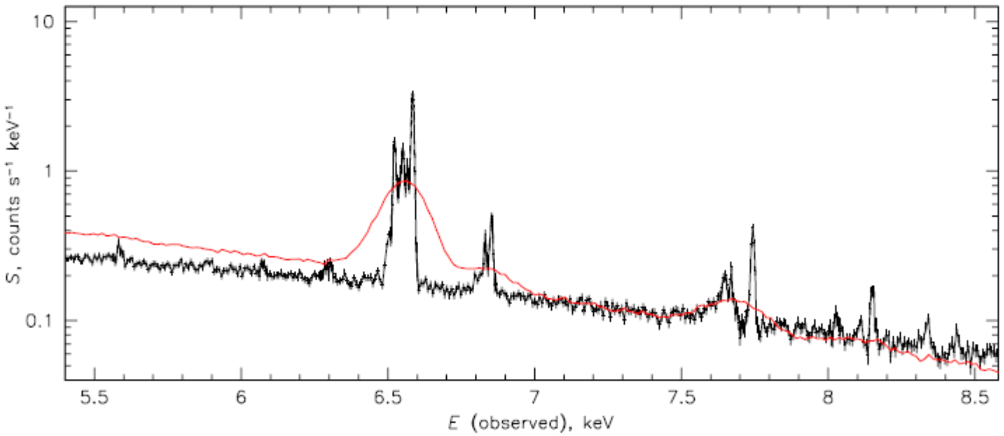

Fig E1. SXS spectrum of the full field overlaid with a CCD spectrum of the same region. The CCD is the Suzaku XIS (red line); the difference in the continuum slope is due to differences in the effective areas of the instruments.

Fig. 2. Spectra of FeXXV He-α, XXVI Lyman α and XXV He-β from the outer region. Gaussian fits have been made to lines with energies (marked in red) from laboratory measurements in the case of He-lil XXV, and theory in the case of Fe XXVI (see Extended Data Table 1 fo details) with the same velocity dispersion, except for the He-α reso line which was allowed to have its own width. Instrumental broade with (blue line) and without (black line) thermal broadening are indicated. The redshift is the cluster value to which the data were se

calibrated using the He-α lines. The strongest resonance (w), intercombination (x,y) and forbidden (z) lines are indicated.

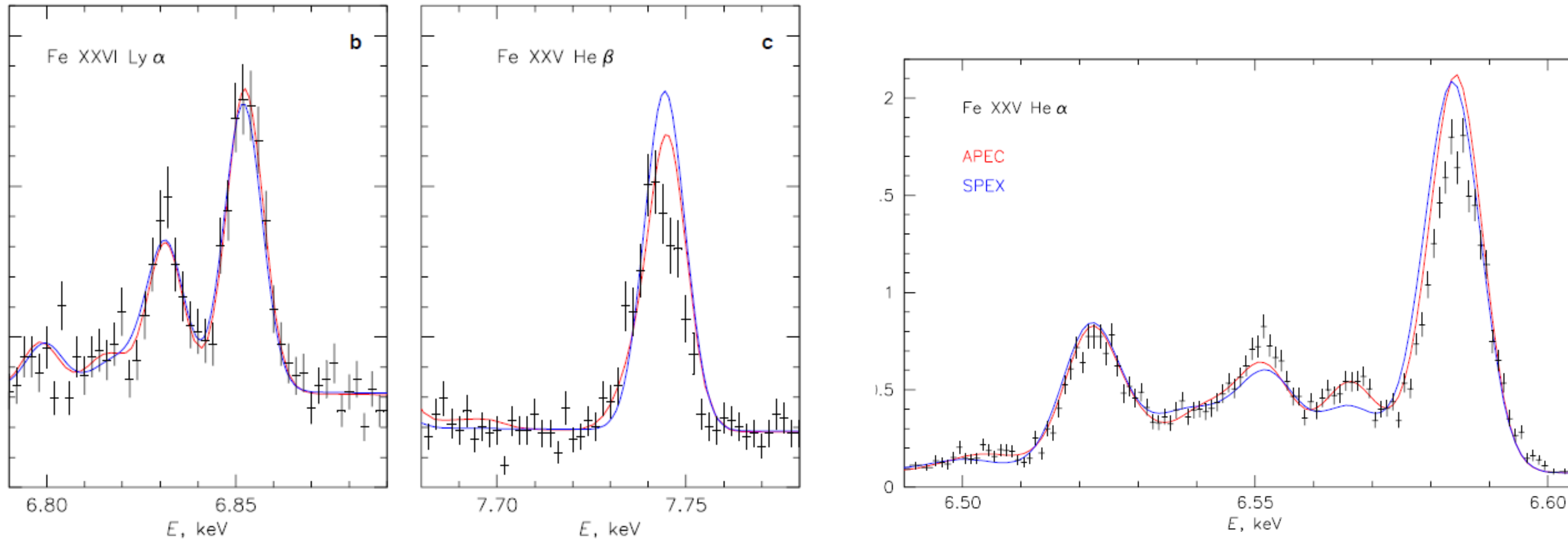

2. The iron line complexes from the outer region compared with fit models. These have been obtained from various emission line bases typically used in the literature. The spectra were modelled ingle temperature, optically thin plasma in collisional ionisation brium using either APEC/ATOMDB 3.0.3 (ref 16; red) or SPEX ef. 17; blue). We determined the best-fit model by fitting the ni spectrum from the outer 23 pixels in the energy range 6.4-8 excluding the Fe He-α resonance line and Ni He-α line complex. btain consistent best-fit parameters, with both APEC and SPEX predicting a temperature of 4.1±0.1 keV. The iron to hydrogen abundances are 0.62±0.02 from APEC and 0.74±0.02 from SPEX, relative to Solar values[31]. The line broadening obtained from APEC, 146±7 km/s, is smaller than the best-fit SPEX value of 171±7, although both values are consistent with the line broadening obtained by fitting a set of Gaussians (the result presented in the main body of the paper). Apart from the Fe He-α w line affected by resonance scattering, both emission line models presented here currently have difficulty reproducing the measured Fe He-α intercombination lines as well as the exact position of the Fe He-β line. This motivates the model-independent approach to determining the line widths adopted in the manuscript.

Dispersion velocity calculation

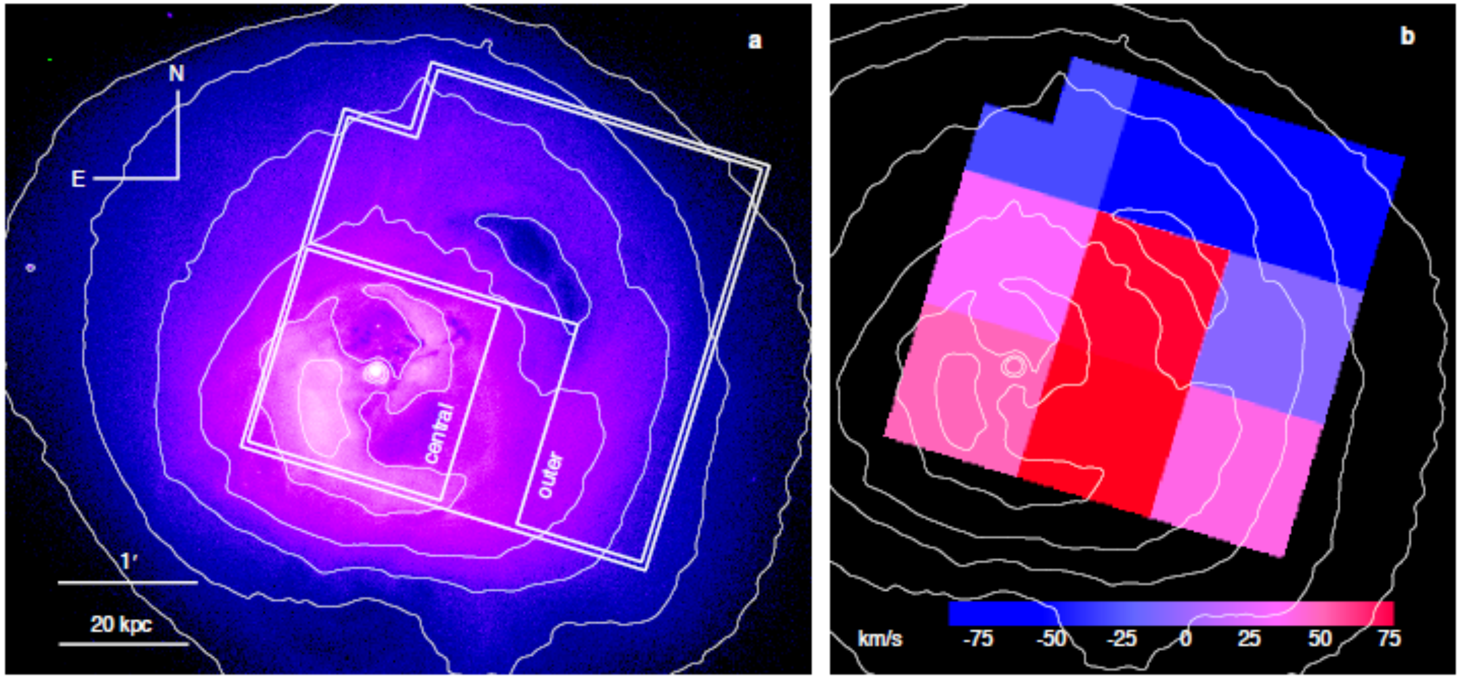

Fig. 3. The region of the Perseus cluster and velocity field viewed by the SXS.
a) The field of view of the SXS overlaid on a Chandra image. The nucleus of NGC1275 is seen as the white dot with inner bubbles N and S. A buoyant outer bubble lies NW of the centre of the field. A swirling cold front coincides with the second contour in from the outside. The central and outer regions are marked.

b) The bulk velocity field across the imaged region. Colors show difference from the velocity of the central galaxy NGC 1275 (who redshift is z=0.01756); positive difference means gas receding fa than the galaxy. The one arcmin pixels of the map correspond approximately to the angular resolution, but are not entirely independent (see Extended Data). The calibration uncertainty on velocities in individual pixels and in the overall baseline is 50 km (Δz=0.00017).

Looking inside: Methods

Gain corrections and calibration

Gain scales for each pixel were measured in ground calibration using a series of fiducial x-ray lines at several detector heat sink temperatures (a single spectral energy reference is sufficient to determine the effective detector temperature and thus the appropriate gain curve to use). As the heat-sink temperature varies, the gain of each pixel tracks the gain change in the separate calibration pixel that is continuously illuminated by a dedicated ^{55}Fe source. However, time-varying differential thermal loading of the pixels changes their gains by different factors. Thus, use of the gain history of the calibration pixel alone can be insufficient to correct the gain scale of the main array.

⇨ Two-stage approach: gain history + science observation

Dispersion velocity derivation process:

- Heliocentric correction
- Weak background line
- Additional scale factor
- Fixed energy resolution
- 10% uncertainty in instrumental broadening
- Small statistical error for scale factor (90% confidence level)
- No velocity variation across field (≥20 kpc scales)

Effects of angular resolution:

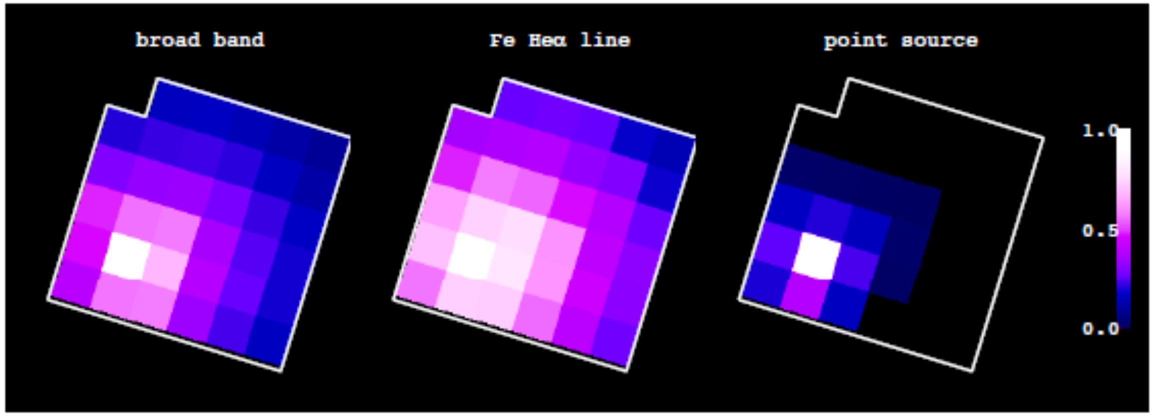

The telescope point spread function (PSF) has a 1.2' half-power diameter (HPD) as measured during ground calibration. This means that regions used for spectral extraction get photons not only from the corresponding cluster regions in the sky, but also from the surrounding regions. The PSF image is shown in right panel of Fig. E5, centered on the SXS pixel that contains the cluster peak.

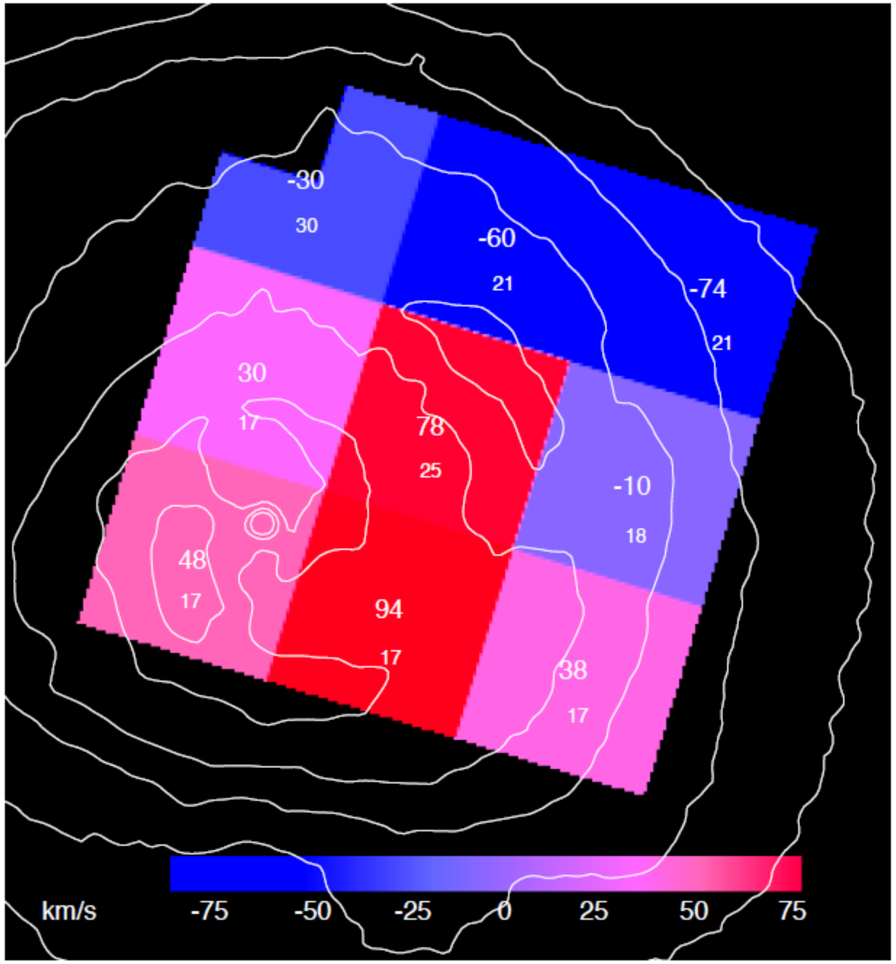

Fig E6. The line-of-sight gas velocities are overlaid on a deep Chandra image^33. The contours increase by a factor of 1.5. The 90% errors in the figure are statistical only; our estimate of the calibration uncertainty in individual pixels is 50 km/s. Heliocentric correction has been applied. Velocities are shown relative to that of NGC1275, whose redshift is z=0.01756^37

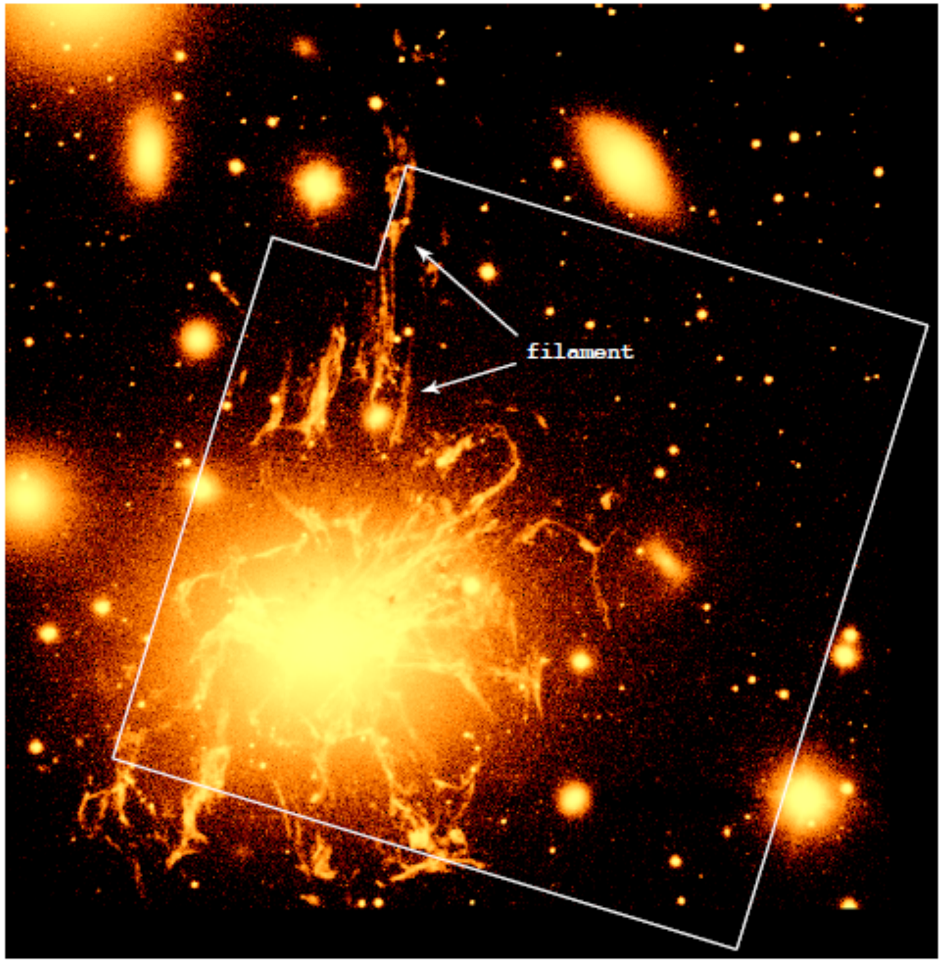

Fig E7. The SXS field is overlaid .on the cold gas nebulosity surrounding NGC1275. The image shows Hα emission[32]. The radi velocity along the long Northern filament measured from CO data decreases, South to North (within the SXS field of view), from abo +50 to -65 km/s. This is similar to the trend seen in the SXS veloc map (E6).

Pointing

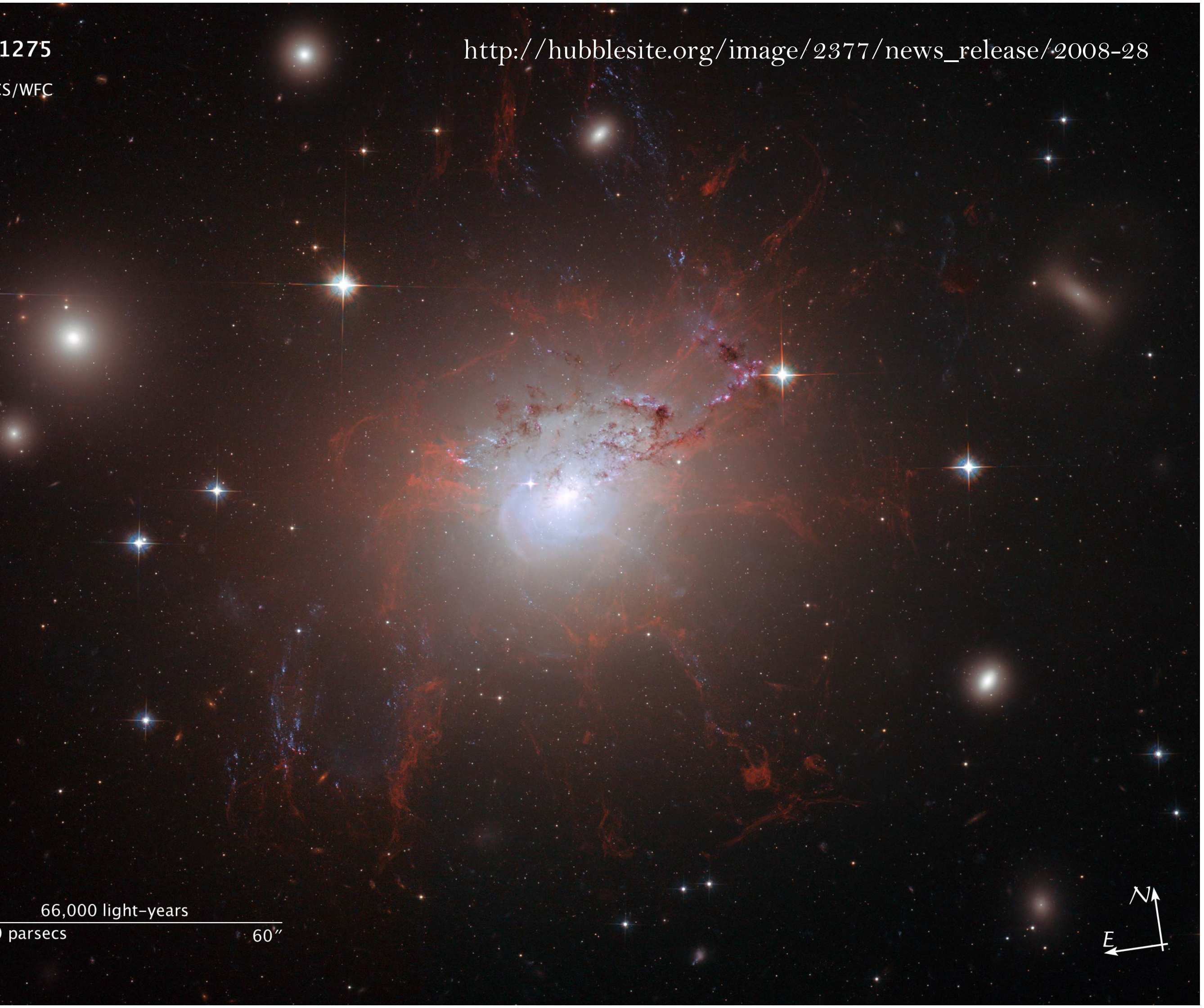

For this early observation, accurate pointing direction of the spacecraft was not available. We therefore assumed that the observed brightness peak in the SXS image is the AGN in NGC1275. The resulting uncertainty of the sky coordinates should be less than 15". The peak of the source determined in short time intervals revealed a small drift of the source in the detector image, within the above coordinate uncertainty. It causes image smearing that is insignificant compared to the PSF scattering effect.

Conclusions from observation: different hypothesis

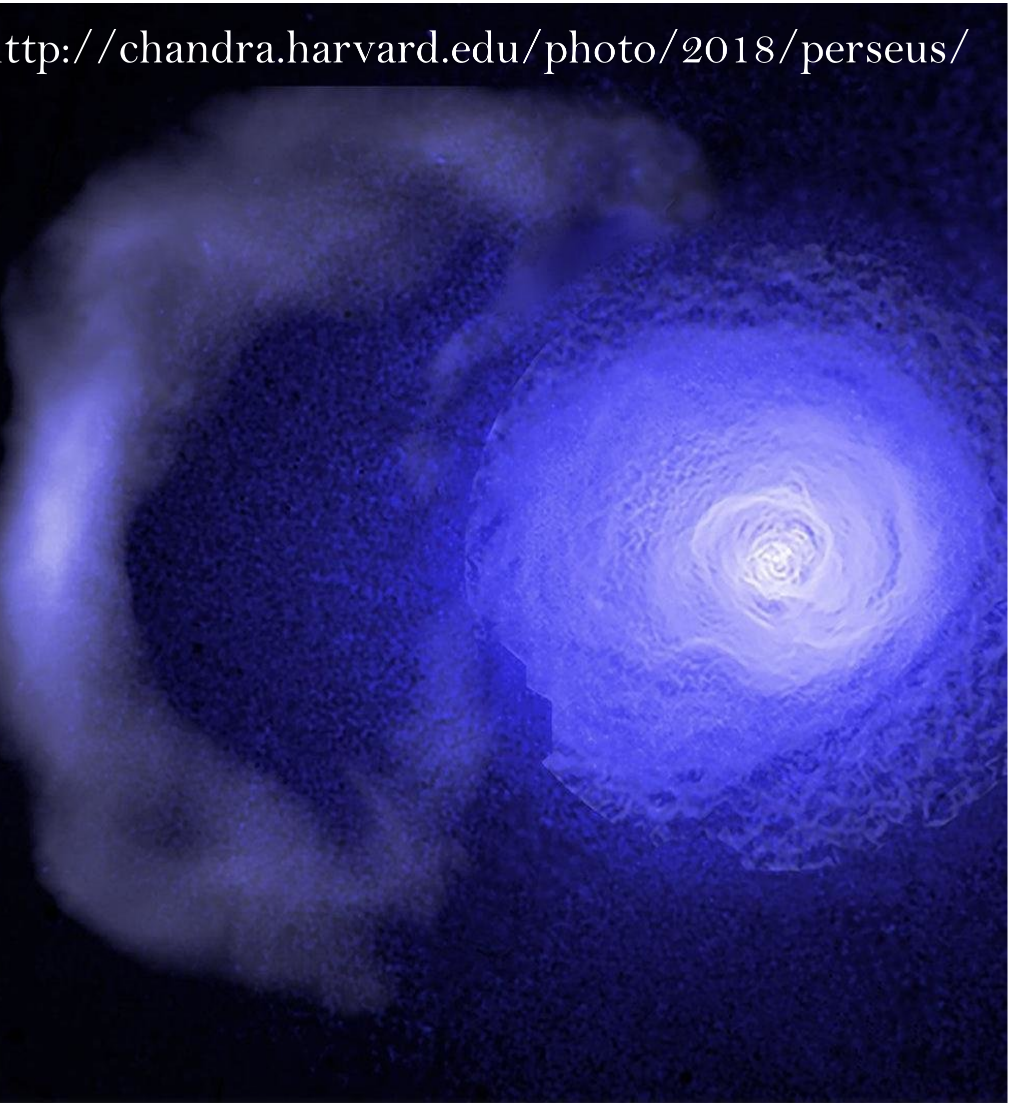

NGC1275 hosts a giant (80 kpc wide) molecular nebula seen in CO and Hα of total cold gas mass several 10^{10} $M_{\odot}$, which dominate the total gas mass out to 15 kpc radius. The velocities of that gas are consistent with the trend of the SXS bulk shear, suggesting that the molecular gas moves together with the hot plasma. (More details of the X-ray spectra and imaged region are given in Extended Data Figs 1-8.)

The large-scale bulk shear over the observed 60 kpc field is c comparable amplitude to the small-scale velocity dispersion that we derive for the outer region. The dispersion can be du to gas flows around the rising bubble at the centre of the field, a velocity gradient in the cold front contained in this region, sound waves, turbulence or galaxy motions. The large-scale shear could be due to the buoyant AGN bubbles, or sloshing motions of gas in the cluster core that give rise to the cold front.

the observed dispersion is interpreted as turbulence ven on scales comparable with the size of the largest bles in the field (~20-30 kpc), it is in agreement with the level inferred from X-ray surface brightness uations. In this case, our measured velocity dispersion iggests that turbulent dissipation of kinetic energy uld be sufficient to offset radiative cooling. However, ssuming isotropic turbulence, the ratio of turbulent ure to thermal pressure in the ICM is low at 4%. Such velocity turbulence cannot spread far (<10 kpc) across cooling core during the fraction (4%) of the cooling time in which it must be replenished, so the above chanism requires that turbulence be generated in situ hroughout the core. Another process is needed to ransport the energy from the bubbling region. The rved level of turbulence is also sufficient to sustain the ulation of ultrarelativistic electrons giving rise to the o synchrotron mini-halo observed in the Perseus core.

A low level of turbulent pressure and bulk shear, in a region continuously stirred by a central AGN and gas sloshing, is surprising and may imply that ICM turbulence is difficult to generate and/or easy to damp. If true throughout the cluster this is encouraging for total mass measurements, which depend on knowledge of all forms of pressure support, and for cluster cosmology which depends on accurate masses.

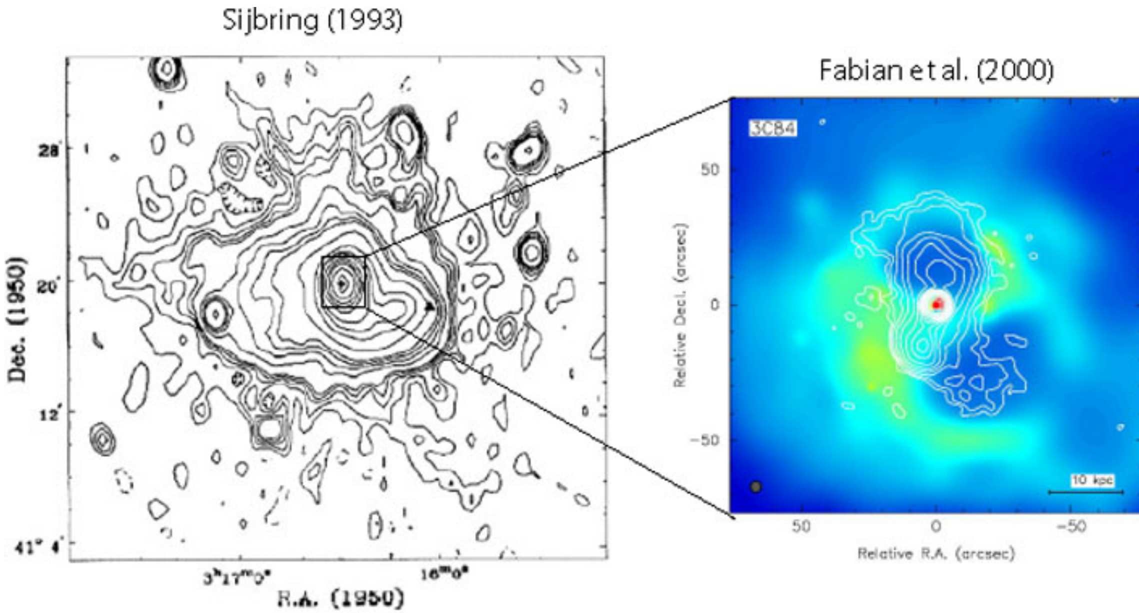

ig: 327 MHz map of the mini-halo in the Perseus Cluster (z = 0.018). The source is centred on the position of the cI alaxy NGC 1275(indicated with a cross). The inset shows radio contours overlaid on the X-ray image of the central ' region of Perseus. The holes evident in the X-ray emission are due to subsonic expansion of the buoyant radio lobe f the central radio galaxy 3C 84 (adapted from Sijbring 1993 and Fabian et al. 2000).

More about Perseus cluster

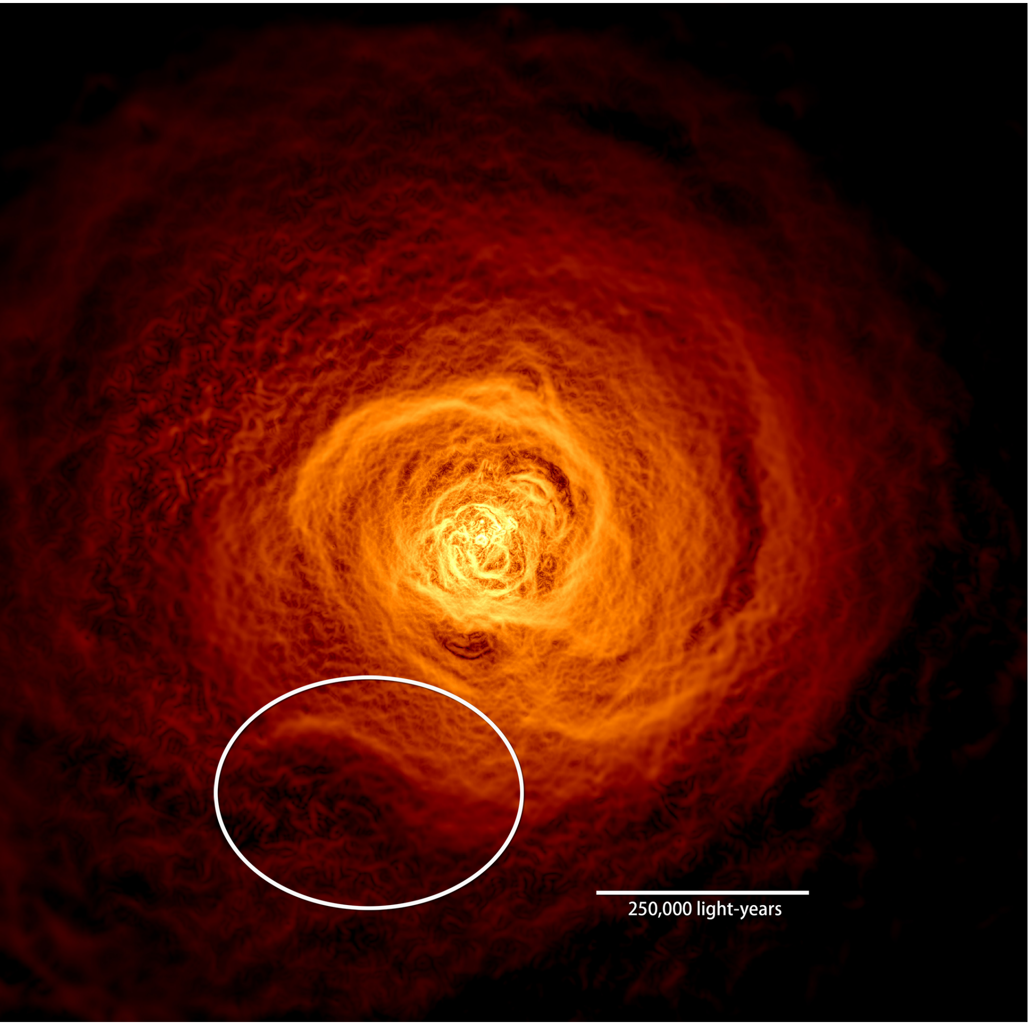

Like all galaxy clusters, most of its observable matter takes the form of a pervasive gas averaging tens of millions of degrees, so hot it only glows in X-rays.
Chandra observations have revealed a variety of structures in this gas, from vast bubbles blown by the supermassive black hole in the cluster's central galaxy, NGC 1275, to an enigmatic concave feature known as the "bay.“
The bay's concave shape couldn't have formed through bubbles launched by the black hole. Radio observations using the [Karl G. Jansky Very Large Array](#) in central New Mexico show that the bay structure produces no emission, the opposite of what scientists would expect for features associated with black hole activity. In addition, standard models of sloshing gas typically produced structures that arc in the wrong direction.

https://www.nasa.gov/feature/goddard/2017/scientists-find wave-rolling-through-the-perseus-galaxy-cluster

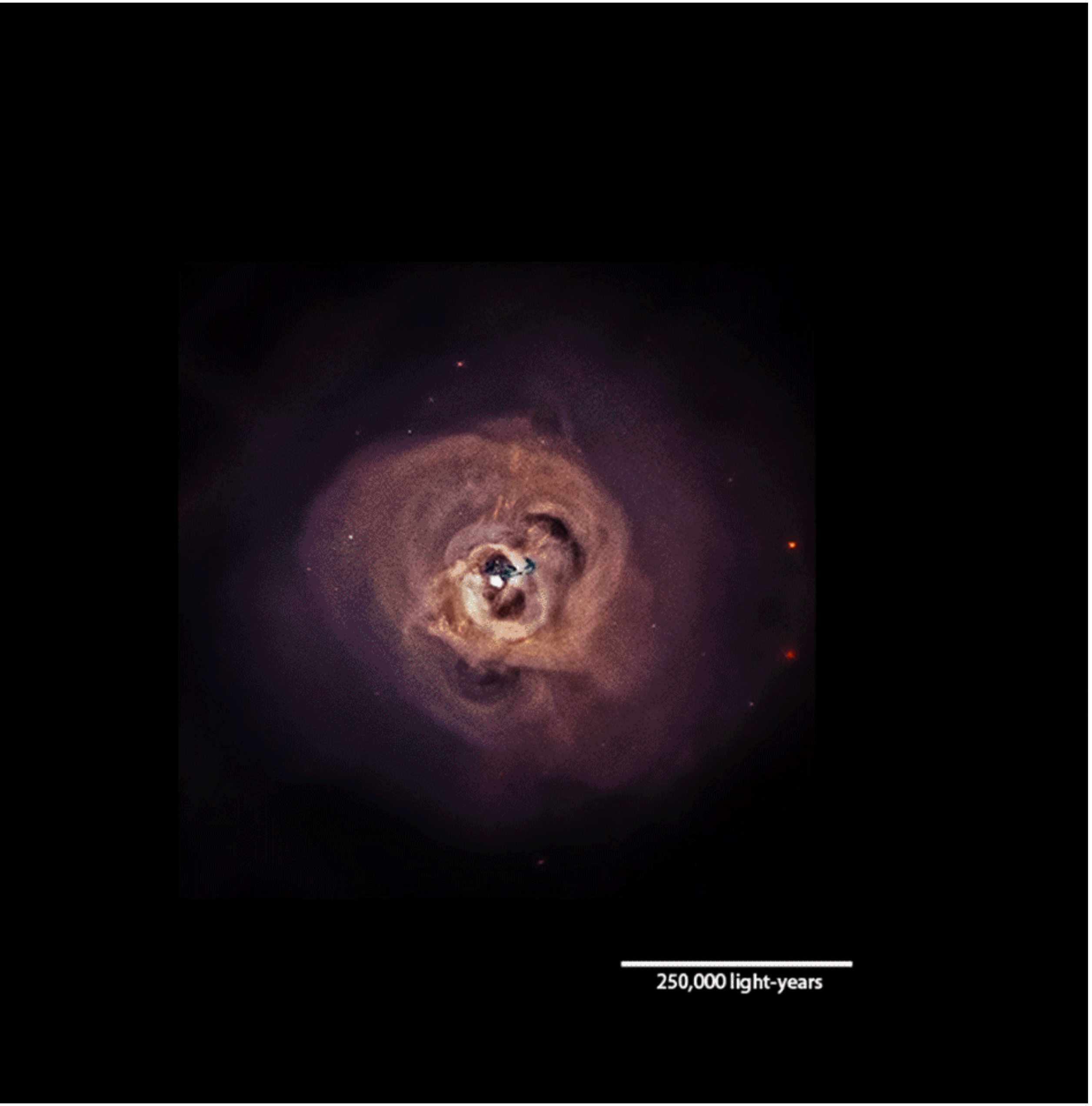

One simulation seemed to explain the formation
the bay. In it, gas in a large cluster similar to Pers
has settled into two components, a "cold" central
region with temperatures around 54 million degr
Fahrenheit (30 million Celsius) and a surroundin
zone where the gas is three times hotter. Then a
galaxy cluster containing about a thousand times
mass of the Milky Way skirts the larger cluster,
missing its center by around 650,000 light-years.
The flyby creates a gravitational disturbance that
churns up the gas like cream stirred into coffee,
creating an expanding spiral of cold gas. After ab
2.5 billion years, when the gas has risen nearly
500,000 light-years from the center, vast waves fo
and roll at its periphery for hundreds of millions
years before dissipating.
These waves are giant versions of Kelvin-Helmho
waves, which show up wherever there's a velocity
difference across the interface of two fluids, such
wind blowing over water. They can be found in t
ocean, in cloud formations on Earth and other
planets, in plasma near Earth, and even on the s